BIOCHEMISTRY
including biophysical chemistry & molecular biology

Article

pubs.acs.org/biochemistry

Influence of Substrate Modification and C-Terminal Truncation on the Active Site Structure of Substrate-Bound Heme Oxygenase from *Neisseriae meningitidis*. A ^{1}H NMR Study

Dungeng Peng,[†] James D. Satterlee,[‡] Li-Hua Ma,[†] Jerry L. Dallas,[§] Kevin M. Smith,[†] Xuhong Zhang,[∥] Michihiko Sato,[⊥] and Gerd N. La Mar*[,†]

[†]Department of Chemistry, University of California, Davis, Davis, California 95616, United States

[‡]Department of Chemistry, Washington State University, Pullman, Washington 99164, United States

[§]NMR Facility, University of California, Davis, Davis, California 95616, United States

[∥]Department of Biochemistry and Molecular Biology, Yamagata University Graduate School of Medical Science, Yamagata 990-9585, Japan

[⊥]Central Laboratory for Research and Education, Yamagata University Faculty of Medicine, Yamagata 990-9585, Japan

Supporting Information

ABSTRACT: Heme oxygenase (HO), from the pathogenic bacterium *N. meningitidis* (*Nm*HO), which secures host iron, shares many properties with mammalian HOs but also exhibits some key differences. The crystal structure appears more compact, and the crystal-undetected C-terminus interacts with substrate in solution. The unique nature of substrate−protein, specifically pyrrole-I/II-helix-2, peripheral interactions in *Nm*HO are probed by 2D ^{1}H NMR to reveal unique structural features controlling substrate orientation. The thermodynamics of substrate orientational isomerism are mapped for substrates with individual vinyl → methyl → hydrogen substitutions and with enzyme C-terminal deletions. *Nm*HO exhibits significantly stronger orientational preference, reflecting much stronger and selective pyrrole-I/II interactions with the protein matrix, than in mammalian HOs. Thus, replacing bulky vinyls with hydrogens results in a 180° rotation of substrate about the α,γ-meso axis in the active site. A "collapse" of the substrate pocket as substrate size decreases is reflected in movement of helix-2 toward the substrate as indicated by significant and selective increased NOESY cross-peak intensity, increase in steric Fe−CN tilt reflected in the orientation of the major magnetic axis, and decrease in steric constraints controlling the rate of aromatic ring reorientation. The active site of *Nm*HO appears "stressed" for native protohemin, and its "collapse" upon replacing vinyls by hydrogen leads to a factor $\sim 10^2$ increase in substrate affinity. Interaction of the C-terminus with the active site destabilizes the crystallographic protohemin orientation by ∼0.7 kcal/mol, which is consistent with optimizing the His207-Asp27 H-bond. Implications of the active site "stress" for product release are discussed.

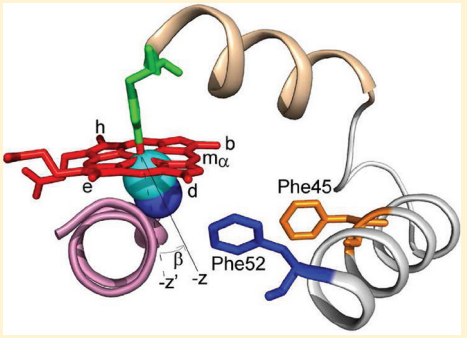

Heme oxygenase (HO) is a widely distributed enzyme that cleaves its natural substrate, hemin, into biliverdin, iron, and CO.[3] In mammals the products serve as a precursor for the potent antioxidant bilirubin, as a source of ∼97% of the required iron, and as a gaseous neuronal messenger.[4−7] The product biliverdin is converted to photosynthetic pigments in plants and cyanobacteria,[8] while in some pathogenic bacteria the primary function is to secure iron.[4,6] All HOs proceed via the same three intermediates—meso-hydroxyhemin, verdoheme, and iron-biliverdin (Scheme 1)—and exhibit significant sequence[4,6] and structural homology with a conserved α-helical fold.[9−15] The stereoselectivity of the meso-cleavage results from distal steric influences that orient first the heme-ligated O_2 and then the activated Fe^{3+}−OOH, toward one meso position, while the distal helix lies sufficiently close to the substrate surface to block the other three meso positions.[9−15] The particular meso position cleaved depends on the seating[9,11,13,14,16−19] of the substrate in the active site which is controlled by propionate−residue salt bridges within a conserved protein matrix; only the α-meso position is cleaved in mammalian HOs.

Crystal structures have shown[9−15] that hemin is bound less tightly in HO substrate complexes than in functional hemoproteins, as evidenced by variable positioning of the key distal helix, high thermal factors, and the presence of multiple and sizable cavities in the vicinity of the active site. Evidence for relatively weak van der Waals interactions between substrate pyrroles I and II (Figure 1) and active site residues is also drawn from ^{1}H NMR data. While only a single substrate orientation is detected in crystals,[9−15] ^{1}H NMR has shown clearly that, for the

Received: June 25, 2011
Revised: August 25, 2011
Published: August 27, 2011

Scheme 1. Identified Intermediates in the Heme Oxygenase Mechanism

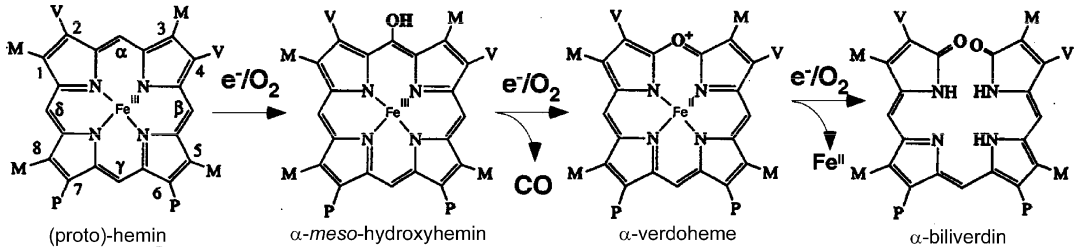

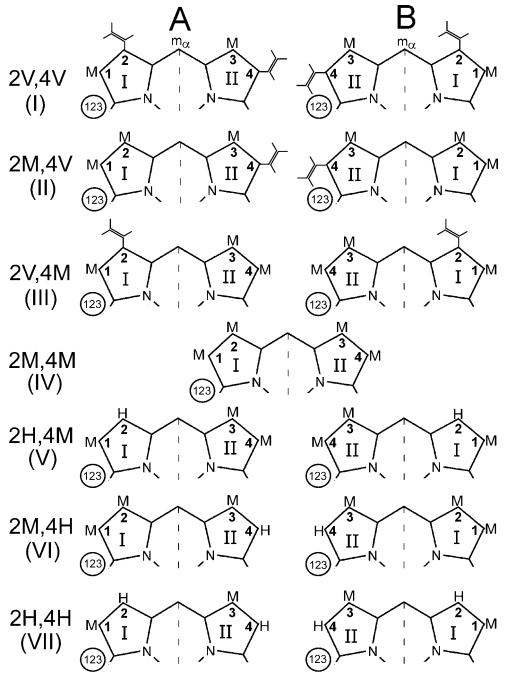

Figure 1. Structures of pyrroles I and II (not shown are pyrroles III and IV which possess conserved methyls at positions 5 and 8 and propionates at positions 6 and 7) for substrates of interest, (2R,4R′)deuterohemins: (i) native protohemin, (2V,4V)DH; (ii) 2-methyl,4-vinyldeuterohemin, (2M,4V)DH; (iii) 2-vinyl,4-methyldeuterohemin, (2V,4M)DH; (iv) 2-fold symmetric 2-,4-dimethyldeuterohemin, (2M,4M)DH; (v) 4-methyldeuterohemin, (2H,4M)DH; (vi) 2-methyldeuterohemin, (2M,4H)DH; (vii) deuterohemin, (2H,4H)DH. The orientation A on the left corresponds to a crystallographic orientation of protohemin,[11,12] while orientation B corresponds to the orientation rotated 180° about the α,γ-meso axis. The 2-fold symmetric (2M,4M)DH is labeled on the basis of the A orientation.

mammalian HOs, the two alternate orientations about the heme α,γ-meso axis (Figure 1) are comparably populated[20−22] in either the resting state or its ligated derivative. Further, the ratio of the two isomers is only weakly altered[20] by substitution of vinyls by hydrogens. In fact, for human HO (hHO), the unique crystal orientation[9] corresponds to the minor isomer in solution.[21] Similar orientational heterogeneity is observed for the two pathogenic bacterial HOs from *Corynebacterium diphtheriae* (*Cd*HO)[17,18,23] and *Pseudomonas aeruginosa* (*Pa*HO).[16,24]

The HO from the pathogenic bacterium *Neisseriae meningitidis* (*Nm*HO) displays significant sequence[6] and structural homology[11,12] to other HOs but, at the same time, exhibits several properties that reflect on unique interactions of the substrate with the protein matrix. On the one hand, the crystal structures indicate[11,12] a more tightly packed active site with fewer and smaller distal cavities than other HOs. On the other hand, solution ^{1}H NMR has shown that *Nm*HO has a stronger orientational preference for the native substrate[2,25,26] and exhibits dynamic line broadening[1] of an aromatic ring in contact with substrate that reflects on steric constraints in the substrate−matrix interaction. These results suggest a more specific and selective interaction between pyrroles I and II with the protein for *Nm*HO than in other HOs. Lastly, the crystallographically undetected[11,12] C-terminal His 207Arg208His209 fragment is observed[25,27] by NMR to interact directly with the active site; NOESY cross-peaks and energy minimization have generated a molecular model.[28,29] Relatively rapid, spontaneous cleavage of the His207-Arg208 peptide bond abolishes the C-terminal interaction and increases the product release[28] rate, thereby implicating the C-terminus as a site for physiological regulation of product release. The contribution of this interaction of the C-terminus with the active site toward the stability of the native *Nm*HO substrate complex is unknown.

We focus here on assessing the influence of substrate size and C-terminal modification on the interaction of the substrate with *Nm*HO and to shed light on the novel structural features of *Nm*HO that exert a significantly stronger substrate orientational preference than in mammalian HOs. The role of the C-terminal interaction with the active site on the substrate contacts with the protein matrix will be similarly explored. The presently documented tendency of the active site *Nm*HO−substrate complex to "collapse" upon decreasing substrate size, and the concomitant increase in substrate affinity, is not apparent in the molecular structure of the native *Nm*HO−substrate complex and may play a role in product extrusion. To this end, we make use of a series of systematically modified substrates where the 2,4-vinyl (V) groups of protohemin are individually replaced by methyls (M), followed by the replacement of these methyls individually by hydrogen (H);[30] the structures of the variable pyrroles I and II are depicted in Figure 1. The influence of the C-terminus on substrate binding is pursued using the previously characterized C-terminal truncation mutants[29] where the three residues, His207Arg208His209, are sequentially deleted and for which the interaction of the C-terminus is minimally perturbed by deleting His209 but is completely abolished upon deletion of Arg208. The azide- and cyanide-inhibited, $S = 1/2$ complexes are ideal candidates for effective and informative 2D NMR characterization.[31] The azide[2,29,32] complex is superior in that it allows direct detection of the contact between the C-terminus and the substrate[29,33] and structurally more closely resembles the bent physiological Fe−O_2 unit.[10,14] The cyanide complex, on the other hand, exhibits electronic/magnetic properties that are much more sensitive to active site perturbations than the azide complex.[25,27,31]

dx.doi.org/10.1021/bi200978g | *Biochemistry* 2011, 50, 8823−8833

MATERIALS AND METHODS

Protein Preparation. Wild-type *Neisseria meningitidis* heme oxygenase (*Nm*HO) and the three C-terminal truncation mutants, desHis209-*Nm*HO (hereafter labeled ΔC1-*Nm*HO), desArg208His209-*Nm*HO (hereafter labeled ΔC2-*Nm*HO), and desHis207Arg208His209-*Nm*HO (hereafter labeled ΔC3-*Nm*HO), are the same as described previously.[25,28,29]

For convenience, we adopt a substrate nomenclature based on deuterohemin (DH), where we explicitly list the substituents at positions 2 and 4, i.e., (2R,4R′)DH (see Figure 1). The seven substrates—protohemin, (2V,4V)DH, 2-methyl,4-vinyldeuterohemin, (2M,4V)DH, 2-vinyl,4-methyldeuterohemin, (2V,4M)DH, 2-,4-dimethyldeutorohemin, (2M,4M)DH, 4-methyldeuterohemin, (2H,4M)DH, 2-methyldeuterohemin, (2M,4H)DH, and deuterohemin, (2H,4H)DH—are the same samples described in detail previously.[30,34] Sample concentrations were determined photometrically. The appropriate hemin was dissolved in 0.1 M NaOH solution, and stoichiometric amounts were added to a *Nm*HO solution 50 mM in phosphate at pH 7.1 at 25 °C. The samples were purified by column chromatography on Sephadex G25 and concentrated using pressure ultrafiltration to yield ∼2−3 mM solutions of *Nm*HO-(2R,4R′)DH-N_3 in H_2O, 50 mM phosphate, 75 mM in azide at pH 7.1. Separate samples of *Nm*HO-(2H,4H)DH-CN and *Nm*HO-(2M,4M)DH-CN were prepared in the same manner with the solution 30 mM in cyanide. A pure ∼1 mM sample of the azide complex of (2V,4V)DH was prepared by dissolving (2V,4V)DH in 0.1 M NaOH in 85% ^1H_2O/15% ^2H_2O ∼56 mM in azide, 81 mM in phosphate; the sample pH was reduced, without precipitation, to ∼7.3 by addition of ^2HCl in ^2H_2O.

NMR Spectroscopy. ^1H NMR data were collected on Bruker AVANCE 500, 600, and 800 spectrometers operating at 500, 600, and 800 MHz, respectively. Reference spectra were collected in ^1H_2O at repetition rates of 1 s^{-1} over 50 ppm; chemical shifts are referenced to 2,2-dimethyl-2-silapentane-5-sulfonate (DSS) through the water resonance. 600 and 800 MHz NOESY spectra[35] (mixing time 40 ms; repetition rate 1.0−2.5 s^{-1} for azide complexes and 1.3 s^{-1} for cyanide complexes) and 500 MHz Clean-TOCSY spectra[36] (to suppress ROESY response; spin lock 25 ms; repetition rate 1.2 s^{-1}) were recorded over a bandwidth of 20 and 44 ppm (NOESY) and 20 ppm (TOCSY) using 512 t1 blocks of 128 and 256 scans, each consisting of 2048 t2 points. 2D data sets were apodized by 30°-sine-squared-bell-functions and zero-filled to 2048 × 2048 data points prior to Fourier transformation.

Magnetic Axes. The orientation of the paramagnetic susceptibility tensor, χ (magnetic axes, x, y, z), relative to the iron-centered reference coordinate system, x', y', z', in Figure 2 was determined for *Nm*HO-(2H,4H)DH-CN, using as input dipolar shifts for residues excluding the distal helix and helix-2 (vide infra), in a manner identical to that described in detail for *Nm*HO-(2V,4V)DH-CN[25] and *Nm*HO-(2M,4M)DH-CN,[27] using $\Delta\chi_{ax} = 2.48 \times 10^{-8}$ m^3/mol and $\Delta\chi_{rh} = -0.58 \times 10^{-8}$ m^3/mol shown to be conserved among His/CN^- ligated hemoproteins.[31,37] In the absence of an isostructural diamagnetic analogue for *Nm*HO, diamagnetic chemical shifts were determined by the ShiftX program[25,27,38] and the crystal structure,[12] to which was added the porphyrin ring current. This procedure yielded nonlabile proton chemical shifts with ±0.25 ppm uncertainties; deviations were random. It has been shown for other HOs[39,40] for which isostructural diamagnetic analogues are available that the magnetic axes determined using alternately the available diamagnetic analogue chemical shifts and the ShiftX program estimates are essentially indistinguishable. Error analysis is described in detail elsewhere.[41] The determined angles β, α, and κ correspond to the tilt of the major magnetic axis (not shown) from the heme normal (z'), the direction of the tilt defined by the angle between the projection of z on the x',y'-plane and the x'-axis, and the position of the in-plane rhombic axes, respectively, as shown in Figure 2.

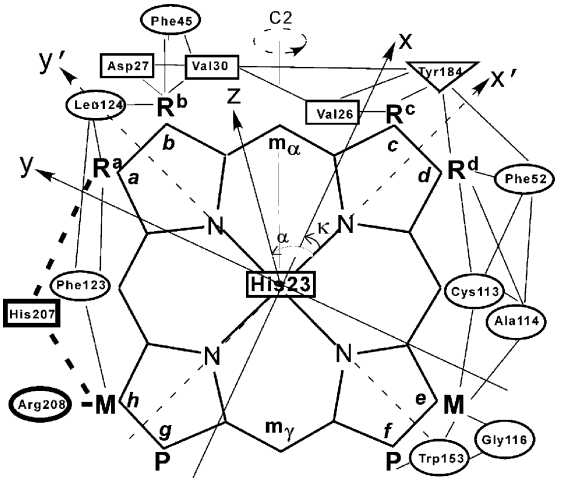

Figure 2. Active site of the *Nm*HO substrate complex depicting the key expected proximal (rectangles), distal (ovals), and equatorial (triangle) residue−substrate and inter-residue dipolar contacts (solid lines) as predicted by the crystal structure[11,12] and observed by ^1H NMR. The positions on the eight pyrrole substituents are labeled not by the conventional numbering of the substrate but by letters a−h defined by the position in the protein matrix. Two contacts not observed in the crystal, but detected by NMR, are the His207 (bold rectangle) C_βHs and ring contacts to methyls at position a and h and the Arg208 (bold oval) C_αH contact to methyl at position h (shown in bold dashed lines). For the native protohemin substrate in the crystal, the substituents 1 → 4 occupy the protein positions corresponding to a → d; conversely, the minor 180°-rotated isomer the substituents 1 → 4 occupy protein positions corresponding to d → a. The reference coordinate system x', y', z' (dotted lines) and the magnetic coordinate system x, y, z (solid lines) are shown where β (not shown) corresponds to the tilt of the major magnetic axes, z, from the substrate normal (z'-axis), α corresponds to the angle between the projection of the major magnetic axis on the x',y'-plane and the x'-axis, and κ corresponds to the in-plane position of the rhombic axis.

RESULTS

Thermodynamics of Substrate Orientational Isomerism. The equilibrium constant for the substrate orientational interconversion, K(B→A) for the native (A in Figure 1) orientation and that rotated 180° about the α,γ-meso axis (B in Figure 1) relates to a difference in the thermodynamic stabilities according to

$$\Delta G^\circ(\mathrm{B} \rightarrow \mathrm{A}) = -RT \ln K(\mathrm{B} \rightarrow \mathrm{A}) \quad (1)$$

with K(B→A) = [A]/[B], where [A] and [B] are the equilibrium populations of the crystallographic (A) and 180°-rotated (B) substrate orientation (Figure 1), as determined from the relative ^1H NMR intensities of resolved methyl peaks in the A to that in the B orientation. Initial reaction of substrate[25] and *Nm*HO leads to ∼1:1 orientational disorder of the substrate about the α,γ-meso axis; the half-life for

dx.doi.org/10.1021/bi200978g | *Biochemistry* 2011, 50, 8823−8833

equilibration to the more stable orientation is ~1.5 h at 25 °C and pH ~7.1. All ^{1}H NMR studies were performed on completely equilibrated complexes.

The effect of replacing the vinyls of *Nm*HO-(2V,4V)-DH-N_3 with methyls, one at a time, to yield *Nm*HO-(2M,4V)-DH-N_3, *Nm*HO-(2V,4M)-DH-N_3, and *Nm*HO-(2M,4M)-DH-N_3 is illustrated in Figure 3A–D. Methyls and single protons for

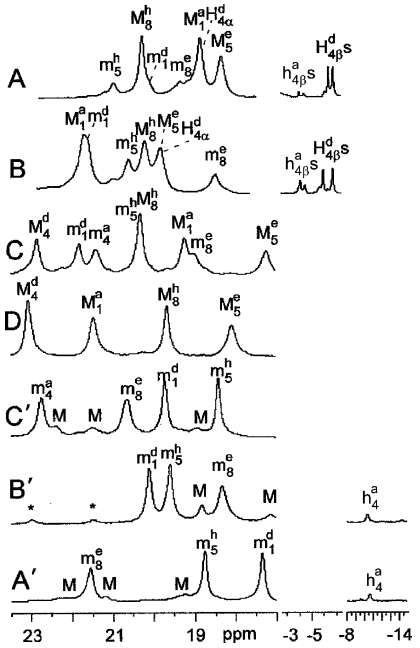

Figure 3. Resolved portions of the 600 MHz ^{1}H NMR spectra, in ^1H_2O, 50 mM in phosphate, 75 mM in azide, pH 7.1 at 25 °C for (A) native *Nm*HO-(2V,4V)DH-N_3, (B) *Nm*HO-(2M,4V)DH-N_3, (C) *Nm*HO-(2V,4M)DH-N_3, (D) *Nm*HO-(2M,4M)DH-N_3, (C′) *Nm*HO-(2H,4M)DH-N_3, (B′) *Nm*HO-(2M,4H)DH-N_3, and (A′) *Nm*HO-(2H,4H)DH-N_3. Substrate peaks are labeled M^j_i, H^j_i (m^j_i, h^j_i) for methyl groups, single proton peaks for the isomer with substrate orientation A (B) as in the crystal structure (180°-rotated about the α,γ-meso axis); subscript *i* corresponds to the substrate positions 1–8 (positions 1–4 depicted in Figure 1), and superscript *j* corresponds to the protein matrix positions *a*–*h* occupied by that substituent, depicted in Figure 2. Asterisks denote peaks for the cleaved *Nm*HO complexes that form over time.

the crystallographic (180°-rotated) orientation isomer are labeled M^j_i, H^j_i (m^j_i, h^j_i), where subscript *i* corresponds to the positions on the substrate (positions 1–8) and superscript *j* corresponds to the position in the protein matrix (positions *a*–*h*) that the substituent occupies, as defined in Figure 2. The native (2V,4V)DH complex exhibits two sets of resonances (Figure 3A). One set corresponds to the previously assigned[25] major isomer with orientation A, whereas a second set of minor isomer peaks, m^j_i, h^j_i, will be shown (vide infra) to correspond to orientation B. The isomer ratio (A/B) is 5:1. Both *Nm*HO-(2M,4V)-DH-N_3 (Figure 3B) and *Nm*HO-(2V,4M)-DH-N_3 (Figure 3C) exhibit heterogeneity with a ratio of major to minor isomers of 13:5 and 7:5, respectively. The relevant thermodynamic parameters are listed in Table 1. The 2-fold symmetric (2M,4M)-DH complex can yield only a single isomer, as found in Figure 3D (for convenience, we number the (2M,4M)-DH positions on the basis of the numbering in native (2V,4V)DH (Figure 1)).

The stepwise replacement of the hydrogens with methyls for the deuterohemin complex is shown in Figure 3A′–C′,D.

Table 1. Thermodynamic Parameters for *Nm*HO-(2R,4R′)DH-N_3 Substrate Orientational Isomerism about the α,γ-Meso Axis[a]

substrate[b] 2R,4R′	enzyme	K(B→A)[c]	$\Delta G°$(B→A)[d]
2V,4V	WT *Nm*HO	5.0 ± 0.4	−1.0 ± 0.1
2M,4V	WT *Nm*HO	2.6 ± 0.2	−0.57 ± 0.05
2V,4M	WT *Nm*HO	1.4 ± 0.2	−0.20 ± 0.09
2H,4H	WT *Nm*HO	0.050 ± 0.013	1.8 ± 0.2
2M,4H	WT *Nm*HO	0.25 ± 0.03	0.55 ± 0.6
2H,4M	WT *Nm*HO	0.020 ± 0.04	0.42 ± 0.13
2V,4V	ΔC1-*Nm*HO	4.8 ± 0.3	−0.94 ± 0.03
2V,4V	ΔC2-*Nm*HO	18 ± 3	−1.7 ± 0.1
2V,4V	ΔC3-*Nm*HO	18 ± 3	−1.7 ± 0.1

[a]Samples in ^1H_2O 50 mM phosphate, 75 mM in azide, pH ~7.1 at 25 °C. [b]As illustrated in Figure 1. [c]For the equilibrium orientation B → orientation A in Figure 1. [d]In kcal/mol, determined from eq 1 at 25 °C.

*Nm*HO-(2H,4H)DH-N_3 (Figure 3A′) exhibits a dominant (~95%) isomer. Replacement of 2H- with 2M- yields two isomers in the ratio of 1:4 (Figure 3B′), while replacing only the 4H- with 4M- yields two isomers in the ratio of 1:5 (Figure 3C′). The thermodynamic parameters for the orientational equilibria are listed in Table 1.

Assignment Protocols. Determining the substrate orientation demands the assignment of specific methyls/hydrogens on the substrate (Figure 1) and the active site amino acids with which they are in dipolar contact, as described by the positions *a*–*h* in Figure 2. We emphasize the azide complex of substrates identified in Figure 1 since they allow ready quantitation of the relative populations of the two substrate orientations (vide infra). The cyanide complexes are considered primarily for *Nm*HO-(2H,4H)DH-CN and *Nm*HO-(2M,4M)DH-CN (vide infra). For significantly populated (>30%) orientational isomers, the complete substrate signals are readily assigned by standard procedures following the pattern of dipolar connectivities about the substrate periphery, as detailed previously for both cyanide and azide *Nm*HO complexes of (2V,4V)DH[2,25] and (2M,4M)DH.[27,29] The NOESY cross-peak pattern of vinyls also establish their orientation relative to the substrate; a *cis* (*trans*) orientation places the vinyl $H_\beta s$ ($H_\alpha s$) close to the methyl on the same pyrrole. The major isomers of *Nm*HO-(2V,4V)DH-X (X = CN, N_3) have been shown[2,25] to possess *cis* orientations for both vinyls in solution, as found in the crystal.[11,12] Chemical shifts for substrate substituents 2R/4R′ = methyl/vinyl and methyl/hydrogen for azide complexes are provided in Supporting Information Tables S1 and S2, respectively. Similar data for cyanide complexes with 2R = 4R′ are listed in Table S3.

The necessary residue assignments are readily obtained from standard α-helical dipolar contacts among TOCSY-detected spin systems over a range of temperatures, which serve as the "third dimension". Such data have been presented in detail previously for several substrate complexes of *Nm*HO with both azide and cyanide ligands.[2,25,27,29] Hence, very limited 2D data are presented. These data provide the definitive assignments for helical fragments Thr19-Val26, Phe52-Thr54, Tyr112-Gly116, Phe123-Phe125, Arg140-Ala142, and Ala180-Tyr184. Chemical shifts of active site residues for azide and cyanide complexes with 2R = 4R′ are provided in Supporting Information Tables S4 and S5, respectively. Similar data for azide complexes with 2R ≠ 4R′ are provided in Table S6. The two key residues in the

protein matrix that uniquely determine substrate orientation are Phe123 (α-helical fragment Phe123-Phe125) and Cys113 (α-helical fragment Tyr112-Gly116), which are in contact with heme substituents at positions *a*, *h* and *d*, *e*, respectively, (Figure 2). For isomers with small populations (<30%), the upfield vinyl $H_{4\beta}$ or pyrrole H_4 dipolar contact to the low-field methyl (or the strong intermethyl contact for two methyls on the same pyrrole) is readily detected, and the methyl contact to Cys113 or Phe123 determines orientation.

Orientation of Substrates with Vinyl Groups. The minor isomer of native *Nm*HO-(2V,4V)DH-N_3 reveals (Figure 3A) two resonances at high field for 4-vinyl $h_{4\beta}$s that exhibit the characteristic NOE to the low-field 4 h_α and to a methyl, m_5, in contact with Phe123 (not shown; see Supporting Information Figure S1). The contact to the Cys113 $C_\alpha H$ identifies m_8, identifying the remaining methyl as m_1, which in turn exhibits a cross peak to $h_{2\alpha}$. These connections confirm the B orientation of the minor isomer and, at the same time, establish that both the 2-vinyl and 4-vinyl groups each possess the *trans* orientation. The strong vinyl $h_{4\beta}$ to the Phe123 ring shows that the vinyl is rotated toward the distal side.

2D NMR data (not shown, see Supporting Information Figure S2) on *Nm*HO-(2M,4V)DH-N_3 reveal the strongly coupled M_2 and M_1 (with M_1 in contact to M_8) and with M_1/M_8 in contact with Phe123, which confirm the A orientation for the major isomer with the 4-vinyl at position *d* in the *cis* configuration. For the minor isomer, the $h_{4\alpha}$-m_3 cross-peaks and the $h_{4\beta}$ cross-peaks to Phe123 confirm the B orientation with the 4-vinyl group at position *a* with a *trans* orientation. The major isomer of *Nm*HO-(2V,4M)DH-N_3 allows complete assignment of the substrate (not shown; see Supporting Information Table S2), and the NOESY cross-peaks of M_5/M_4 to Cys113 $C_\alpha H$ and M_8/M_1 to Phe123 establish the A orientation for the major isomer with the 2-vinyl group displaying a *cis* orientation at the same protein position *b* as the native substrate. For the minor isomer, the strong NOESY cross-peaks of m_4 to both m_3 and Phe123 dictate the B orientation. The m_1 to the vinyl $h_{2\alpha}$ NOESY cross-peak establishes a *trans* orientation for the 2-vinyl at protein matrix position *c*. Thus, vinyls at the crystallographic positions *b* and *d* exhibit *cis*, while those at positions *a* and *c* exhibit *trans* orientations. The observed vinyl orientation for each substrate is depicted in Figure 1.

Orientation of Substrates with Pyrrole Hydrogens. The NOESY data for the major isomer of *Nm*HO-(2H,4H)-DH-N_3 in Figure 4 reveal the key m_1 to m_8 cross-peak and the cross-peak of both methyls to Cys113 $C_\alpha H$, dictating that the major isomer has the "reversed" orientation B (Figure 1). The line widths[a] of the Tyr184 ring $C_\varepsilon H$ averaged[1] resonance is very strongly reduced compared to that in either the (2M,4M)DH or (2V,4V)DH complexes[25,27] (not shown, see Supporting Information Figure S3). For this complex, as well as in the case of the other substrates,[2,25,27] we observe both the His207 $C_\beta H_2$ and Arg208 $C_\alpha H$ NOESY cross-peaks to the methyl at position *h*, confirming that the substrate in each complex interacts with the C-terminus in a manner similar to that described for the native (2V,4V)DH complexes.[2,29] Similar NOESY data for *Nm*HO-(2M,4H)DH-N_3 and *Nm*HO-(2H,4M)DH-N_3 (data not shown) also confirm that the major isomer corresponds to the B orientation (Figure 1).

The ^{1}H NMR spectra for *Nm*HO-(2V,4V)DH-CN and *Nm*HO-(2H,4H)DH-CN each exhibit primarily a dominant (~20:1) orientation (not shown, see Supporting Information Figure S4),; with $\Delta G^\circ = -1.8$ and +1.8 kcal/mol, respectively.

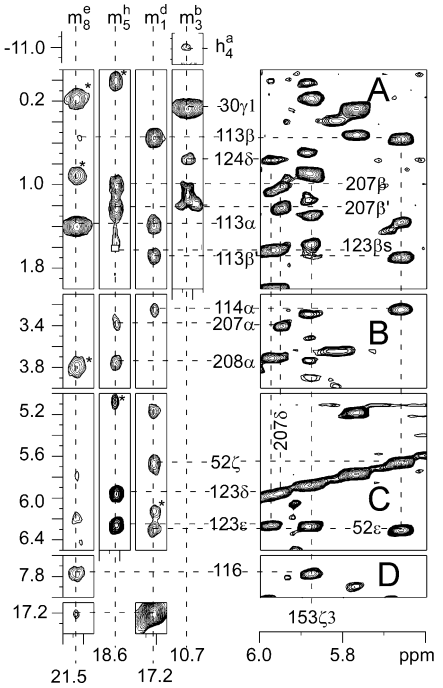

Figure 4. Portions of the 600 MHz ^{1}H NMR NOESY spectrum (spectral width 37 ppm and repetition rate 2.5 s^{-1} (left four columns) and spectral width 20 ppm repetition rate 1.5 s^{-1} (right column)) of *Nm*HO-(2H,4H)DH-N_3 in H_2O, 50 mM phosphate, 75 mM azide, pH 7.1, at 25 °C illustrating the residue contacts to the substrate that establish that the orientation of the major isomer (95%) as that rotated by 180° about the $\alpha-\gamma$-meso axis (B orientation in Figure 1) relative to that of native protohemin.

For the former complex, the A orientation has been confirmed.[25] NOESY data on the latter complex (not shown) reveal a dominant B orientation, as for the azide complex (vide infra). Chemical shifts for the substrate and active site residues are provided in Supporting Information Tables S3 and S5, respectively.

Influence of C-Terminal Deletions on Orientational Equilibrium and Substrate Affinity. Figure 5 illustrates the resolved upfield spectral window where the assigned[29] 4-vinyl H_βs resonate for WT *Nm*HO-(2V,4V)DH-N_3 and the ΔC1-, ΔC2-, and ΔC3-*Nm*HO truncation mutants. Deletion of the C-terminal His209 has only a minimal effect on the A/B isomer ratio (Figure 5B and Table 1). However, both ΔC2- and ΔC3-*Nm*HO-(2V,4V)DH-N_3 exhibit similarly significantly increased K(B→A) from 5 to 18, indicating that abolishing the interaction of the C-terminus with the active site favors the A orientation found in crystals[11,12] (thermodynamic parameters listed in Table 1).

The ^{1}H NMR spectrum of a solution 1.0 mM *Nm*HO, 1.0 mM ΔC2-*Nm*HO, and 1.1 mM (2V,4V)DH, in the presence of excess azide, exhibits the methyl peaks for *Nm*HO-(2V,4V)DH-N_3 and ΔC2-*Nm*HO-(2V,4V)DH-N_3 with comparable (±10%) integrated intensities (not shown; see Supporting Information Figure S5), dictating that in azide complexes the affinity for substrate is essentially the same in the WT and ΔC2-*Nm*HO complex.

Active Site Structural Perturbations upon Substrate Modification. The primary equatorial contacts of pyrrole I and II substituents[11,12] are with the side chains of helix-2 that includes the residues Phe45-Phe52, as illustrated in Figure 6. An assessment of the proximity of this helix to the substrate

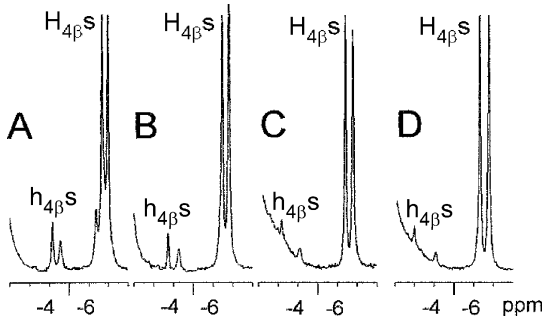

Figure 5. Upfield portion of the 600 MHz ^{1}H NMR spectra showing the 4-vinyl $H_{4\beta}s$ and $h_{4\beta}s$ for the major A and the minor B substrate orientations, respectively, for (A) native *Nm*HO-(2V,4V)DH-N_3, (B) ΔC1-*Nm*HO-(2V,4V)DH-N, (C) ΔC2-*Nm*HO-(2V,4V)DH-N_3, and (D) ΔC3-*Nm*HO-(2V,4V)DH-N_3 in 50 mM phosphate, 75 mM azide, pH 7.1, at 25 °C.

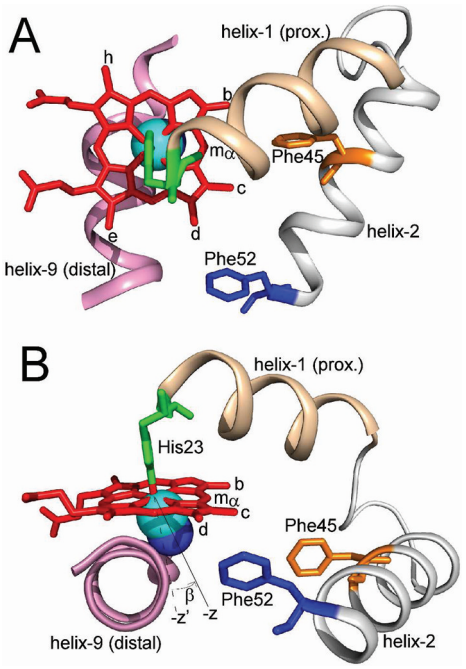

Figure 6. Schematic drawing of the portions of the proximal helix-1 (His23-Val33; beige), helix-2 (Lys39-Phe52; gray), and distal helix-9 (Tyr112-Phe123; pink) relative to the substrate (red), as observed in crystal structure (Protein Data Bank crystal coordinates ID 1P3V).[11,12] Methyls at the three active site positions *b*, *c*, and *d* are labeled. Shown are the positions of the side chains for the axial His23 (green) and two key aromatic contacts with pyrroles I/II, Phe45 (orange) and Phe52 (dark blue), as well as the expected tilt of the Fe−CN unit (light blue spheres) in the direction of the α-meso position, m_α (as inferred from the tilt of the major magnetic axes of χ). The normal to the substrate, −*z*′, and the major magnetic axis, *z*, that is determined by the steric tilt of the Fe−CN unit from the heme normal, as given by the angle β, are also depicted.

requires an invariant probe (same rigid functional group in two complexes to be compared). Inspection of the orientations of the major isomers of (2V,4V)DH (A in Figure 1) and (2H,4H)DH (B in Figure 1), and the unique orientation of (2M,4M)DH, shows that the only conserved probes are methyls at active positions *b* and *d* (Figure 2) for the (2M,4M)DH and (2H,4H)DH complexes and methyls at positions *a* and *c* for (2V,4V)DH and (2M,4M)DH complexes.

The active site structure (PDB crystal coordinates ID 1P3V) in Figure 6 depicts a Phe45 ring which cannot move closer to the methyl at position *b* solely by side chain reorientation. Similarly, the ring of Phe52 could move closer to the methyl at position *d* simply by side chain reorientation, but not to the methyl at position *c*. The methyls at positions *b* and *c* are resolved only in the cyanide complex[25,27] while methyls *a* and *d* are resolved only in the azide complex.[2,32,42] The most informative spectra are those for the cyanide complexes.

Figures 7A and 7B show the NOESY slices (collected and processed under identical spectral conditions) through methyls

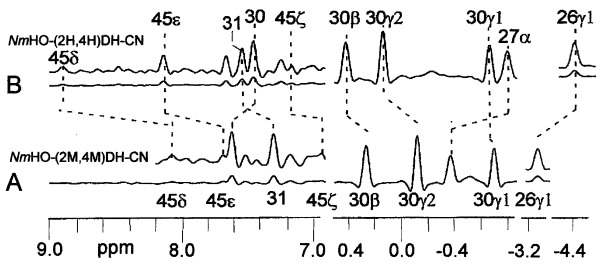

Figure 7. 600 MHz NOESY slices through the conserved methyl at active site position *b* (Figure 2) for (A) *Nm*HO-(2M,4M)DH-CN and (B) *Nm*HO-(2H,4H)DH-CN in ^1H_2O, 50 mM phosphate, 75 mM azide, pH 7.1, and 25 °C. The spectra were collected under identical conditions (spectral width 40.0 ppm, repetition rate 1.5 s^{-1}) and plotted on the same absolute scale. The essentially conserved cross-peak intensities to proximal helix residues Val26, Asp27, and Val30 upon replacing methyls by hydrogens at positions 2 and 4 are noted, as is the significant increase in the intensity of the cross-peak to the Phe45 $C_\varepsilon H$ for the (2H,4H)DH relative to (2M,4M)DH substrate.

at position *b* for the (2M,4M)DH and the (2H,4H)DH cyanide complexes, respectively. NOESY data for both complexes readily identify the expected[11,12] relatively strong contacts of the protons of Val26, Asp27, and Val30 (Figure 7; see also Supporting Information Figure S6). For the *Nm*HO-(2M,4M)DH-CN complex, a very weak NOESY cross-peak is observed to the $C_\varepsilon H$ of Phe45 (Figure 7A), as expected from the crystal structure. It is noted that the NOESY cross-peak intensities for Val26, Asp27, and Val30 to the substrate methyl are conserved upon replacing the substrate methyl with a hydrogen at positions 2 and 4, indicating conserved configuration for the proximal helix relative to the substrate. On the other hand, the intensity of the substrate methyl to the Phe45 $C_\varepsilon H$ increases (Figure 7B) by a factor of 3−4 for the reduced substrate size. The increase in magnitude of the Phe45 $C_\varepsilon H$ NOE for the (2M,4M)DH complex indicates a movement by the Phe45 ring, and hence helix 2, ∼1 Å closer to the substrate upon replacing 2,4 methyl with 2,4 hydrogen, a shift comparable to the expected reduction of the substrate size. A NOESY cross-peak between the methyl at position *b* and the Phe52 ring in the (2V,4V)DH complex is neither predicted[11,12] nor observed[25] by ^{1}H NMR. The detection of a weak-to-moderate intensity cross-peak (not shown) between the Phe52 $C_\varepsilon H$ and the methyl at position *c* in the (2M,4M)DH cyanide complex[27] confirms a similar movement of helix-2 closer to the substrate upon replacing vinyls by methyls. The M^d NOESY slices in the azide complexes exhibit the expected cross-peaks to three aromatic rings (Phe52, Phe181, and Tyr184) (not shown); pairwise degeneracies of the ring signals preclude a meaningful dissection of changes in cross-peak intensity.

Effect of Substrate Modification on the Magnetic Axes in Cyanide Complexes. The hyperfine shifts for

dx.doi.org/10.1021/bi200978g | *Biochemistry* 2011, 50, 8823−8833

nonligated active site residues arise solely from the dipolar interaction and are determined by the orientation/anisotropy of the paramagnetic susceptibility tensor, χ, and the position of the residues in the active site.[31,43] Systematic changes in active site dipolar shift pattern for a largely conserved molecular structure infer changes in the orientation of χ, which can be indirectly related to small systematic structural changes in the active site.[15,22,31,44]

Replacement of the two vinyls in (2V,4V)DH, first with methyls and subsequently with hydrogens, in azide complexes produces only very small chemical shift changes for active site residues (in particular, for the proximal helix), but always in the order vinyl, methyl, hydrogen. Hence, the orientation of χ is essentially conserved with variable 2−4-substituents in azide complexes. The variation in dipolar shift with 2R,4R for cyanide complexes, on the other hand, is both large in magnitude and exhibits a systematic change in pattern with the shifts changing always in the order vinyl, methyl, hydrogen (not shown, see Supporting Information Tables S3 and S4).

Previous determinations[25,27] of the orientation of χ for the (2V,4V)DH and (2M,4M)DH cyanide complexes have shown that the tilt of the major magnetic axis, z, from the heme normal, z', is 8 ± 1° in the former but increased to 12 ± 1° for the latter substrate, with the direction of tilt, α = 250 ± 15°, and the rhombic axes, κ = 40 ± 10°, largely conserved (the angle β is more clearly depicted in Figure 6). Comprehensive 2D NMR assignments of *Nm*HO-(2H,4H)DH-CN (not shown; see Supporting Information Table S6) allow the present determination of the orientation of χ for *Nm*HO-(2H,4H)DH-CN. The magnitude of the dipolar shifts significantly exceeds the likely small changes in the porphyrin ring currents upon changing the 2,4-substituents, allowing the use of the same diamagnetic chemical shift references as for the (2V,4V)DH complex. This procedure leads to conserved α = 230 ± 15°, and rhombic axes, κ = 34 ± 15°, but with significantly increased tilt, β = 16 ± 1° (not shown, see Supporting Information Figure S7). Hence, the magnitude of the tilt of the major magnetic axis of χ in cyanide complexes with substituent size increases in the order H > M > V, with the direction of tilt largely conserved. Since the Fe−CN vector correlates with the −z-axis (Figure 6B), the Fe−CN is tilted toward the α-meso position.[15,25,27,31,44]

Influence of Substrate Modification on Substrate Affinity. The ^{1}H NMR spectrum of a solution 1.0 mM in WT *Nm*HO, 1.1 mM in (2H,4H)DH and 1.0 mM in (2V,4V)DH, in the presence of excess azide, exhibits the expected resolved methyl peaks for both *Nm*HO-(2H,4H)DH-N_3 and *Nm*HO-(2V,4V)DH-N_3, but in an intensity ratio of ∼20:1. This dictates[b] that, assuming similar aggregation[45] or nonspecific interaction of the "free" substrate with the intact *Nm*HO−substrate complex, the substrate affinity for (2H,4H)DH is a factor >10^2 greater than for the native (2V,4V)DH (not shown, see Supporting Information Figure S8).

DISCUSSION

Electronic/Magnetic Properties of the Substrate. The pattern of substrate dominant contact shifts (see Supporting Information Tables S1−S3) adheres to that expected[31,46] for the respective orbital ground states for the low-spin azide[2,42] and cyanide[31,47] complexes, large low-field contact shifts for methyls, propionate, and vinyl H_αs, and high-field contact shifts for vinyl H_βs at positions 1, 4, 5, 8[2,3,6,7] for the azide (cyanide) complexes. The in-plane 90° rotation of the orbital hole is due to the fact that it is determined by the orientation of the axial imidazole and the bent Fe−N═N═N planes which are perpendicular to each other.[14,42] There is also smaller asymmetry among the methyl shifts at positions 1, 4, 5, 8 in the azide complexes reflecting, in significant part, the in-plane asymmetry induced by the asymmetric arrangement of the 2 and 4 substituents in the free substrate.[48]

The relative insensitivities of the dipolar shifts of non-coordinated active site residues to substrate modification in azide complexes, in contrast to the strong sensitivity for cyanide complexes, are again consistent with expectations. Variable distal steric interactions necessarily lead to variable tilt of the Fe−C vector in cyanide complexes because the Fe−CN unit is linear.[15] The azide ligand, like molecular oxygen, is bent upon ligation to iron, such that distal steric interactions control primarily the direction of the plane of the bent ligand, but not the Fe−N tilt.[15]

Substrate Orientational Preference. The contribution to the stabilization of the crystallographic orientation for a given substrate ($\Delta G°$ in Table 1) is approximately additive for the 2- and 4-positions, and the influence at the 2- and 4-positions is comparable for hydrogens and slightly larger for the 4- than 2-vinyl (Table 1). The conversion of the more common vinyl *cis* orientations in the crystallographic *b* and *d* positions (Figure 2), to the less common *trans* orientation for active site positions *a* and *c*, is readily rationalized by steric influences predicted by the crystal structures.[11,12]

The preference for the vinyl vs methyl and methyl vs hydrogen positions in the active site can be combined such that the binding-free energy for substrate in the crystallographic (A orientation) increases (becomes more negative) in the order H > M > V at each of the active site positions *a* and *c*, while for positions *b* and *d*, the binding-free energy is reversed in the order V > M > H. The similar effect of the 2-vinyl and 4-vinyl to methyl substitutions on orientational preference argues against a significant electronic influence of specific vinyl−protein interactions in controlling orientation. Electronic inductive effects may modulate protein contact with the substrate π system but in the order vinyl, hydrogen, methyl.[49] However, for the three azide complexes this pattern correlates with an increase in the binding free energy as the size of the pyrrole I/II substituent, and hence size of substrate, decreases. The binding free energies for a given orientation for the substrates (2V,4V)-DH and (2H,4H)DH differ by ∼2.8 kcal/mol (Table 1).

Thermodynamic data for substrate orientation as cyanide complexes are available only for (2H,4H)-DH and (2V,4V)DH, with $\Delta G°$ = +1.8 and −1.8 kcal/mol, respectively. For (2H,4H)DH the "reversed" orientation is comparably stabilized ($\Delta G°$ = 1.8 kcal/mol) for the alternate exogenous ligands. However, for (2V,4V)DH, the A orientation is stabilized by ∼0.8 kcal/mol more in the cyanide than azide complex. The difference in orientational preference for (2V,4V)DH in cyanide and azide complexes likely arises from a stronger interaction of the former substrate with the protein matrix forced by the steric tilt of the Fe−CN unit.[14,15]

The Role of the C-Terminus Interaction with Substrate. For each of the substrates, the interaction of the C-terminus with the active site can be confirmed by the NOESY cross-peaks of a weakly relaxed His backbone (His207) to substituents at the active site positions *a* and *h* and of a weakly relaxed and upfield dipolar-shifted C_αH (Arg208) to the methyl at position *h* in a manner essentially indistinguishable from that reported previously for (2V,4V)DH and (2M,4M)DH complexes with both azide and cyanide

ligands.[2,25,27−29] The spectra in Figure 5 and the thermodynamic data in Table 1 show that $\Delta G°$ is conserved upon deletion of His209; this deletion has been shown[29] to retain the interaction of the C-terminus with the active site. The subsequent deletions of first Arg208, and then His207, which have been shown[29] to abolish the interaction of the C-terminus with the active site, leads to a ∼0.7 kcal/mol stabilization of the crystallographic (A in Figure 1) orientation of (2V,4V)DH, although the overall substrate affinity is unaltered.

An H-bond between the His207 peptide NH and the proximal helix Asp27 carboxylate has been proposed[28,29] for the structure of the C-terminus, and it was noted that the out-of-plane orientation of the 2-vinyl group at position *b* sterically interfered with the optimal orientation of the Asp27 carboxylate. The increased population of the B orientation, which places a vinyl at position *a* and a methyl at position *b*, upon the interaction of the C-terminus with the active site can be viewed as a contribution to stabilizing the His207 to Asp27 H-bond. In any case, the significant effect on the relative stabilities of the two substrate orientations establishes the importance of the crystallographically undetected[11,12] interaction of the C-terminus with the active site.

Active Site Structural Accommodation to Substrate Modification. It was noted above that the orientation of the (2V,4V)DH, (2M,4H)DH, and (2H,4H)DH substrate follows the pattern that places the smallest substituent at each of the four active site positions *a*−*d* in Figure 2. This directly implies that the size of the substrate cavity depends on substrate size. A "collapse" of the substrate pocket size upon reduction of the size of the substrate is supported by observations of the movement of two helices relative to the substrate. Figure 6 depicts the relative positions of substrate and portions of the helical backbones for the proximal helix-1, helix-2 (through residues His23-Phe52), and the distal helix spanning the substrate, (Tyr112-Phe123).[11,12] The expected tilt of the Fe−CN unit toward the α-meso position is also shown.

The significant increase, upon replacing (2M,4M)DH with (2H,4H)DH, in the NOESY cross-peak intensity between the Phe45 $C_\varepsilon H$ to the common methyl at the crystallographic[11,12] position *b*, as well as the appearance of a significant NOESY cross-peak between the Phe52 $C_\varepsilon H$ and methyl at position *c* upon replacing vinyls by methyls, indicate that helix-2 moves ∼1 Å closer to the substrate upon reducing the size of the 2,4-substituents.

The tilt of the major magnetic *z*-axis in cyanide complexes reflects the magnitude and direction of the steric tilt of the linear Fe−CN unit, as confirmed by the observation of a ∼20° tilt toward the α-meso position by both ^{1}H NMR[44] and crystallography[15] in a mammalian HO cyanide complex. The observed increase in the tilt angle, β, from 8° for the (2V,4V)DH to 12° for the (2M,4M)DH,[27] and to 16° for the (2H,4H)DH cyanide complexes, indicates that the distal helix backbone, which is the origin of the steric interference for the tilt,[15] moves ∼0.2 Å for vinyl to methyl and methyl to hydrogen replacements. Hence, the distal helix moves only a small fraction of the movement of helix 2 toward the α-meso position (or the proximal helix moves toward the γ-meso position) as the size of the pyrrole I/II substituents decrease in size.

The available data do not distinguish whether the distal helix or substrate move relative to the enzyme center of mass; however, it can be expected that a movement of helix-2 toward the substrate upon replacing methyls by hydrogens at positions 2 and 4 can result in a small movement of the proximal helix in the same direction, and this movement would result in an increased tilt due to steric interaction with the distal helix. It has been noted in mammalian HOs that the replacement of a bent ligand like azide[14] with a linear ligand like cyanide[15] results in a large steric tilt for the Fe−CN unit that causes a movement of the proximal helix, setting a precedent for a correlation between the degree of tilt of the exogenous ligand and translation of the proximal helix.

The helix-2 side chain Gln49 and His53 provide important H-bonds to ordered water molecules implicated in the catalytic mechanism.[7,10−12,14,15] Both the His53 and Glu49 labile protons exhibit significant (>0.3 ppm) shift changes with 2R,4R in both the azide (Table S4) and cyanide (Table S5) complexes. While changes in the orientation of χ complicate the interpretation of these shift changes for the cyanide complex, the conserved orientation of χ for azide complexes clearly shows that these selective shift changes for Gln49 and His53 reflect increases in H-bond strength as the size of the substituent is reduced. Hence, there is a coupling mechanism between the 2,4 positions and the distal pocket of the enzyme.

^{1}H NMR determination of the relative substrate affinities of *Nm*HO for (2V,4V)DH and (2H,4H)DH in the azide complexes shows (not shown, see Supporting Information Figure S8) that the substrate affinity increases[4] by a factor >10^2 upon replacing 2,4-vinyls with 2,4-hydrogens. Thus, the substrate binding free energy is increased (more negative) by ∼2.8 kcal/mol for the smaller substrate. This increased stability can be attributed, at least in part, to the "collapse" of the substrate pocket upon decrease in substrate size. A useful view is that the active site structure is "stressed" for native (2V,4V)DH and is "relaxed" for the smaller (2H,4H)DH. The reduction of the line width[2] of the Tyr 184 $C_\varepsilon H$ signal averaged by 180° ring flips in the order V > M > H (not shown, see Supporting Information Figure S3) confirms a tightly clamped (2V,4V)DH in the "stressed" active site that is sequentially relaxed upon decreasing the size of the 2,4 substituents.

Comparison with Other Heme Binding Proteins. The very strong effect of substrate substitution upon the heme orientational preference (about its α,γ-meso axis) clearly distinguishes *Nm*HO from mammalian HOs. For mammalian HOs, the alternate orientations are comparably populated for both native (2V,4V)DH and (2H,4H)DH.[20−22] The much stronger selectivity between the two substrate orientations in *Nm*HO arises from increased hydrophobic interactions between the substrate and the protein matrix, in particular at the pyrrole I/II interface. The more compact active site structure of *Nm*HO complexes has been deduced[11,12] by observations of fewer and smaller vacancies in its crystal structure in comparison to structures of other HOs. For mammalian HOs, cleavage of the substrate ring leaves a bound iron−biliverdin product in a pocket that is slightly larger and less constrained than previously occupied by the substrate.[14,15] Hence, the substrate pocket of mammalian HOs appears to be stabilized for a size that only loosely holds the substrate. In contrast, the present data support a much tighter substrate pocket for *Nm*HO−substrate complexes that is "stressed" for native (2V,4V)DH, in that there are significant constraints on the substrate. Moreover, decreasing the substrate size permits collapse of the active site to a size that much more strongly binds a smaller substrate.

The significantly increased stabilization of the complex with the smaller (2H,4H)DH relative to native (2V,4V)DH in *Nm*HO is in strong contrast to substrate binding studies of globins. Native (2V,4V)DH and synthetic (2H,4H)DH globins exhibit the same dominant orientation about the α,γ-meso axis,[48] but the affinity for (2H,4H)DH relative to native

(2V,4V)DH is *reduced*[50] (instead of increased as for *Nm*HO) by a factor >10^2. The well-formed heme cavity size in globins[51] apparently cannot similarly collapse to bind the former hemin as strong as the latter.

Functional Implications. A peculiar and characteristic property of HOs in general is that the product, iron−biliverdin, exhibits a spontaneous off-rate (~0.03 s^{-1} for mammalian HO[52]) too slow to support a physiological process. For mammalian HOs, the release of the toxic biliverdin is circumvented by the formation of a transient 1:1 complex with biliverdin reductase (BVR), whose binding at the exposed heme edge[52,53] strongly accelerates product release. The BVR analogue in pathogenic bacteria has not been identified, and the toxicity of biliverdin is not likely as high as in mammals.[4,6] The ^{1}H NMR characterized[2,25,27−29] interaction of the C-terminus of the active site, which is not detected in crystals,[11,12] has been shown to modulate product release rate,[28] and it has been proposed[29] that the C-terminal structural motif may serve as a recognition site for an outer-membrane transporter protein[4] which docks at the exposed heme edge. The present results suggest an additional mechanism. Thus, the "stressed" *Nm*HO substrate pocket, upon cleavage of the macrocycle, may "collapse" in size so as to distort the open macrocycle and facilitate its extrusion. Unfortunately, crystal structures for product complexes of pathogenic bacterial have not yet been reported.

■ ASSOCIATED CONTENT

Supporting Information

Eight figures, NOESY spectra for minor isomer of *Nm*HO-(2V,4V)DH-N_3, and *Nm*HO-(2V,4M)DH-N_3, NOESY slices through Val26-Tyr184 ring for *Nm*HO-(2*R*,4*R*)DH-N_3 with 2R = 4R = vinyl, methyl, and hydrogen, NOESY spectra for *Nm*HO-(2M,4M)DH-CN/*Nm*HO(2H,4H)DH-CN, NMR spectra of *Nm*HO-(2R,4R)DH-CN with 2R = 4R = vinyl, hydrogens, NMR spectra for mixture of *Nm*HO-(2V,4V)DH-N_3/ΔC2-(2V,4V)DH-N_3, magnetic axes for *Nm*HO-(2H,4H)DH-CN, and NMR spectra of a mixture of *Nm*HO-(2V,4V)DH-N_3 and *Nm*HO-(2H,4H)DH-N_3) and six tables (chemical shifts for substrate for azide complexes with methyl/vinyl substituted substrate and methyl/hydrogen substituted substrate and for cyanide complexes with substrates with 2R = 4R and chemical shifts for active site residues for azide complexes with 2R = 4R′, 2R ≠ 4R′ and cyanide complexes with 2R = 4R′). This material is available free of charge via the Internet at http://pubs.acs.org.

■ AUTHOR INFORMATION

Corresponding Author

*E-mail: lamar@chem.ucdavis.edu. Phone: 530-752-0958. Fax: 530-752-8995.

Funding

This research was supported by grants from the National Institutes of Health, GM62830 (G.N.L.) and CA132861 (K.M.S.). NMR instrumentation purchase was supported by grants from the National Institutes of Health, RR1973, and the National Science Foundation, DBIO722538.

■ ABBREVIATIONS

DSS, 2,2-dimethyl-2-silapentane-5-sulfonate; HO, heme oxygenase; hHO, human heme oxygenase; *Nm*HO, *Neisseria meningitidis* heme oxygenase; ΔC1-*Nm*HO, Des-His209-*Nm*HO; ΔC2-*Nm*HO, Des-Arg208His209-*Nm*HO; ΔC3-*Nm*HO, Des-His207Arg208His209-*Nm*HO; BVR, biliverdin reductase; NOESY, two-dimensional nuclear Overhauser spectroscopy; TOCSY, two-dimensional total correlation spectroscopy; ROESY, rotating frame two-dimensional nuclear Overhauser spectroscopy; *Cd*HO, *Corynebacterium diphtheriae* heme oxygenase; *Pa*HO, *Pseudomonas aeruginosa* heme oxygenase; (2V,4V)DH, 2-vinyl,4-vinyldeuterohemin; (2M,4M)DH, 2-methyl,4-methyldeuterohemin; (2H,4H)DH, 2-hydrogen,4-hydrogendeuterohemin; (2M,4V)DH, 2-methyl,4-vinyldeuterohemin; (2V,4M)DH, 2-vinyl,4-methyldeuterohemin; (2M,4H)-DH, 2-methyl,4-hydrogendeuterohemin; (2H,4M)DH, 2-hydrogen,4-methyldeuterohemin.

■ ADDITIONAL NOTES

[a]The line width is reduced at elevated temperature and is greater at 800 than 600 MHz and hence represents dynamic line broadening in the fast-exchange limit.[1] The larger line width contribution to the Tyr184 averaged C_εH than C_δH signals is consistent with the results of previously published magnetic axes[2] which predict only a ~0.1 ppm shift difference for the individual C_δHs, but a ~0.8 ppm shift difference for the individual C_εHs. Since the magnetic axes (dipolar shifts) are conserved with 2R,4R for azide complexes, the reduced exchange broadening directly correlates with a faster ring reorientation in the order H > M > V.

[b]The details of the extraction of the information from the peak intensities are given in Figure S8.

■ REFERENCES

(1) Sandström, J. (1982) *Dynamic NMR Spectroscopy*, Academic Press, New York.

(2) Ma, L.-H., Liu, Y., Zhang, X., Yoshida, T., and La Mar, G. N. (2009) ^{1}H NMR study of the effect of variable ligand on heme oxygenase electronic and molecular structure. *J. Inorg. Biochem. 103*, 10−19.

(3) Tenhunen, R., Marver, H. S., and Schmid, R. (1969) Microsomal heme oxygenase. Characterization of the enzyme. *J. Biol. Chem. 244*, 6388−6394.

(4) Wilks, A. (2002) Heme Oxygenase: Evolution, Structure, and Mechanism. *Antioxidants Redox Signal 4*, 603−614.

(5) Ortiz de Montellano, P. R., and Auclair, K. (2003) *Heme Oxygenase Structure and Mechanism in The Porphryin Handbook* (Kadish, K. M., Smith, K. M., and Guilard, R., Eds.) pp 175−202, Elsevier Science, San Diego, CA.

(6) Frankenberg-Dinkel, N. (2004) Bacterial Heme Oxygenases. *Antoxidants Redox Signal 6*, 825−834.

(7) Unno, M., Matsui, T., and Ikeda-Saito, M. (2007) Structure and catalytic mechanism of heme oxygenase. *Nat. Prod. Rep 24*, 553−570.

(8) Beale, S. I. (1994) Biosynthesis of open-chain tetrapyrroles in plants, algae, and cyanobacteria. *Ciba Found. Symp. 180*, 156−168.

(9) Schuller, D. J., Wilks, A., Ortiz deMontellano, P. R., and Poulos, T. L. (1999) Crystal structure of human heme oxygenase-1. *Nat. Struct. Biol. 6*, 860−867.

(10) Unno, M., Matsui, T., Chu, G. C., Coutoure, M., Yoshida, T., Rousseau, D. L., Olson, J. S., and Ikeda-Saito, M. (2004) Crystal Structure of the Dioxygen-bound Heme Oxygenase from *Corynebacterium diphtheriae*. *J. Biol. Chem. 279*, 21055−21061.

(11) Schuller, D. J., Zhu, W., Stojiljkovic, I., Wilks, A., and Poulos, T. L. (2001) Crystal structure of heme oxygenase from the Gram-negative pathogen *Neisseria meningitidis* and a comparison with mammalian heme oxygeanse-1. *Biochemistry 40*, 11552−11558.

(12) Friedman, J. M., Lad, L., Deshmukh, R., Li, H. Y., Wilks, A., and Poulos, T. L. (2003) Crystal structures of the NO- and CO-bound

heme oxygenase from *Neisseriae meningitidis* - Implications for O_2 activation. *J. Biol. Chem. 278*, 34654−34659.

(13) Friedman, J., Lad, L., Li, H., Wilks, A., and Poulos, T. L. (2004) Structural Basis for Novel *δ*-Regioselective Heme Oxygenation in the Opportunistic Pathogen *Pseudomonas aeruginosa*. *Biochemistry 43*, 5239−5245.

(14) Sugishima, M., Sakamoto, H., Higashimoto, Y., Omata, Y., Hayashi, S., Noguchi, M., and Fukuyama, K. (2002) Crystal structure of rat heme oxygenase-1 in complex with heme bound to azide: Implication for regiospecific hydroxylation of heme at the *α-meso* carbon. *J. Biol. Chem. 277*, 45086−45090.

(15) Sugishima, M., Sakamoto, H., Noguchi, M., and Fukuyama, K. (2003) Crystal Structures of CO-, CN-, and NO-Bound Forms of Rat Heme Oxygenase-1 (HO-1) in Complex with Heme: Structural Implications for Discrimination between CO and O_2 in HO-1. *Biochemistry 42*, 9898−9905.

(16) Caignan, G. A., Deshmukh, R., Wilks, A., Zeng, Y., Huang, H.-w., Moenne-Loccoz, P., Bunce, R. A., Eastman, M. A., and Rivera, M. (2002) Oxidation of heme to *β*- and *δ*-biliverdin by *Pseudomonas aeruginosa* Heme Oxygenase as a Consequence of an Unusual Seating of the Heme. *J. Am. Chem. Soc. 124*, 14879−14892.

(17) Zhou, H., Migita, C. T., Sato, M., Sun, D., Zhang, X., Ikeda-Saito, M., Fujii, H., and Yoshida, T. (2000) Participation of the Carboxylate Amino Acid Side Chain in Regiospecific Oxidation of Heme by Heme Oxygenase. *J. Am. Chem. Soc. 122*, 8311−8312.

(18) Zeng, Y., Deshmukh, R., Caignan, G. A., Bunce, R. A., Rivera, M., and Wilks, A. (2004) Mixed Regioselectivity in the Arg-177 Mutants of *Corynebacterium diphtheriae* Heme Oxygenase as a Consequence of in-Plane Heme Disorder. *Biochemistry 43*, 5222−5238.

(19) Wang, J., Evans, J. P., Ogura, H., La Mar, G. N., and Ortizde Montellano, P. R. (2006) Alteration of the Regiospecificity of Human Heme Oxygenase-1 by Unseating of the Heme but not Disruption of the Distal Hydrogen Bonding Network. *Biochemistry 45*, 61−73.

(20) Hernández, G., Wilks, A., Paolesse, R., Smith, K. M., Ortiz de Montellano, P.R., and La Mar, G. N. (1994) Proton NMR Investigation of Substrate-bound Heme Oxygenase: Evidence for Electronic and Steric Contributions to Stereoselective Heme Cleavage. *Biochemistry 33*, 6631−6641.

(21) Gorst, C. M., Wilks, A., Yeh, D. C., Ortiz de Montellano, P. R., and La Mar, G. N. (1998) Solution ^{1}H NMR investigation of the molecular and electronic structure of the active site of substrate-bound human heme oxygenase: the nature of the distal hydrogen bond donor to bound ligands. *J. Am. Chem. Soc. 120*, 8875−8884.

(22) Zhu, W., Li, Y., Wang, J., Ortiz de Montellano, P. R., and La Mar, G. N. (2006) Solution NMR study of environmental effects on substrate seating in human heme oxygenase; Influence of polypeptide truncation, substrate modification and axial ligand. *J. Inorg. Biochem. 100*, 97−107.

(23) Li, Y., Syvitski, R. T., Chu, G. C., Ikeda-Saito, M., and La Mar, G. N. (2003) Solution ^{1}H NMR investigation of the active site molecular and electronic structures of the substrate-bound, cyanide-inhibited bacterial heme oxygenase from *C. diphtheriae*. *J. Biol. Chem. 279*, 6651−6663.

(24) Fujii, H., Zhang, X., and Yoshida, T. (2004) Essential Amino Acid Residues Controlling the Unique Regioselectivity of Heme Oxygenase in *Pseudomonas aeruginosa*. *J. Am. Chem. Soc. 126*, 4466−4467.

(25) Liu, Y., Zhang, X., Yoshida, T., and La Mar, G. N. (2004) ^{1}H NMR characterization of the solution active site structure of substrate-bound, cyanide-inhibited heme oxygenase from *Neisseria meningitidis*; Comparison to crystal structures. *Biochemistry 43*, 10112−10126.

(26) Liu, Y., Zhang, X., Yoshida, T., and La Mar, G. N. (2005) Solution ^{1}H NMR characterization of the distal H-bond network and the effective axial field in the resting-state, high-spin ferric, substrate-bound complex of heme oxygenase from *N. meningitidis*. *J. Am. Chem. Soc. 127*, 6409−6422.

(27) Liu, Y., Ma, L.-H., Zhang, X., Yoshida, T., Satterlee, J. D., and La Mar, G. N. (2006) ^{1}H NMR study of the influence of hemin vinyl-methyl substitution on the interaction between the C-terminus and substrate and the "aging" of the heme oxygenase from *N. meningitidis*. Induction of active site structural heterogeneity by a two-fold symmetric hemin. *Biochemistry 45*, 13875−13888.

(28) Liu, Y., Ma, L.-H., Satterlee, J. D., Zhang, X., Yoshida, T., and La Mar, G. N. (2006) Characterization of the spontaneous "aging" of the heme oxygenase from the pathological bacterium *Neisseria meningitidis* via cleavage of the C-terminus in contact with the substrate; Implications for functional studies and the crystal structure. *Biochemistry 45*, 3875−3886.

(29) Peng, D., Ma, L.-H., Ogura, H., Yang, E.-C., Zhang, X., Yoshida, T., and La Mar, G. N. (2010) ^{1}H NMR Study of the Influence of Mutation on the Interaction of the C-Terminus with the Active Site in Heme Oxygenase from *Neisseria meningitidis*: Implications for Product Release. *Biochemistry 49*, 5832−5840.

(30) Smith, K. M., and Kehres, L. A. (1983) Syntheses of Methyl Devinylporphyrins Related to Protoporphyrin-IX. Initial Studies on the Mechanism of the Copper (II) Catalyzed Cyclizations of 1′,8′-Dimethyl-a,c-biladienes. *J. Chem. Soc., Perkin Trans. 1*, 2329−2335.

(31) La Mar, G. N., Satterlee, J. D., and de Ropp, J. S. (2000) NMR of Hemoproteins, in *The Porphyrins Handbook* (Kadish, K. M., Smith, K. M., and Guilard, R., Eds.) pp 185−298, Academic Press, San Diego.

(32) Zeng, Y., Caignan, G. A., Bunce, R. A., Rodriguez, J. C., Wilks, A., and Rivera, M. (2005) Azide-inhibited Bacterial Heme Oxygenases Exhibit an S=3/2 $(d_{xz},d_{yz})^3(d_{xy})^1(d_z{}^2)^1$ Spin State: Mechanistic Implications for Heme Oxidation. *J. Am. Chem. Soc. 127*, 9794−9807.

(33) Ma, L.-H., Liu, Y., Zhang, X., Yoshida, T., Langry, K. C., Smith, K. M., and La Mar, G. N. (2006) Modulation of the Axial Water Hydrogen-Bonding Properties by Chemical Modification of the Substrate in Resting State, Substrate-Bound Heme Oxygenase from *Neisseria meningitidis*; Coupling to the Distal H-Bond Network via Ordered Water Molecules. *J. Am. Chem. Soc. 128*, 6391−6399.

(34) Lee, K.-B., La Mar, G. N., Kehres, L. A., Fujinara, E. M., Smith, K. M., Pochapsky, T. C., and Sligar, S. G. (1990) ^{1}H NMR Study of the Influence of Hydrophobic Contacts on Protein-Prosthetic Group Recognition in Bovine and Rat Ferricytochrome b_5. *Biochemistry 29*, 9623−9631.

(35) Jeener, J., Meier, B. H., Bachmann, P., and Ernst, R. R. (1979) Investigation of Exchange Processes by Two Dimensional NMR Spectroscopy. *J. Chem. Phys. 71*, 4546−4553.

(36) Griesinger, C., Otting, G., Wüthrich, K., and Ernst, R. R. (1988) Clean TOCSY for ^{1}H Spin System Identification in Macromolecules. *J. Am. Chem. Soc. 110*, 7870−7872.

(37) Nguyen, B. D., Xia, Z., Yeh, D. C., Vyas, K., Deaguero, H., and La Mar, G. (1999) Solution NMR Determination of the Anisotropy and Orientation of the Paramagnetic Susceptibility Tensor as a Function of Temperature for Metmyoglobin Cyanide; Implications for the Population of Excited Electronic States. *J. Am. Chem. Soc. 121*, 208−217.

(38) Neal, S., Nip, A. M., Zhang, H., and Wishart, D. S. (2003) Rapid and accurate calculation of protein ^{1}H, ^{13}C and ^{15}N chemical shifts. *J. Biomol. NMR 26*, 215−240.

(39) Li, Y., Syvitski, R. T., Auclair, K., Ortiz de Montellano, P. R., and La Mar, G. N. (2003) 1H NMR Investigation of the Solution Structure of Substrate-free Human Heme Oxygenase: Comparison to the Cyanide-inhibited, Substrate-bound Complex. *J. Biol. Chem. 279*, 10195−10205.

(40) Du, Z., Unno, M., Matsui, T., Ikeda-Saito, M., and La Mar, G. N. (2010) Solution ^{1}H NMR characterization of substrate-free *C. diphtheriae* heme oxygenase: Pertinence for determining magnetic axes in paramagnetic substrate complexes. *J. Inorg. Biochem. 104*, 1063−1070.

(41) Xia, Z., Nguyen, B. D., and La Mar, G. N. (2000) The use of chemical shift temperature gradients to establish the paramagnetic susceptibility tensor orientation: implication for structure determination/refinement in paramagnetic metalloproteins. *J. Biomol. NMR 17*, 167−174.

(42) Ogura, H., Evans, J. P., Peng, D., Satterlee, J. D., Ortiz de Montellano, P. R., and La Mar, G. N. (2009) The Orbital Ground

State of the Azide-Substrate Complex of Human Heme Oxygenase Is an Indicator of Distal H-Bonding: Implications for the Enzyme Mechanism. *Biochemistry 48*, 3127−3132.

(43) Bertini, I., and Luchinat, C. (1996) NMR of Paramagnetic Substances. *Coord. Chem. Rev. 150*, 1−296.

(44) Li, Y., Syvitski, R. T., Auclair, K., Wilks, A., Ortiz de Montellano, P. R., and La Mar, G. N. (2002) Solution NMR characterization of an unusual distal H-bond network in the active site of the cyanide-inhibited, human heme oxygenase complex of the symmetric substrate, 2,4-dimethyldeuterohemin. *J. Biol. Chem. 277*, 33018−33031.

(45) Viscio, D. B., and La Mar, G. N. (1978) NMR Studies of Low-Spin Ferric Complexes of Natural Porphyrin Derivatives. 3. Thermodynamics of Dimerization and the Influence of Substituents on Dimer Structure and Stability. *J. Am. Chem. Soc. 100*, 8096−8100.

(46) Shokhirev, N. V., and Walker, F. A. (1998) The Effect of Axial Ligand Plane Orientation on the Contact and Pseudocontact Shifts of Low-spin Ferriheme Proteins. *J. Biol. Inorg. Chem. 3*, 581−594.

(47) Walker, F. A. (2000) Proton NMR and EPR Spectroscopy of Paramagnetic Metalloporphyrin, in *The Porphyrin Handbook* (Kadish, K. M., Smith, K. M., and Guilard, R., Eds.) pp 1−183, Academic Press, Boston.

(48) Kolczak, U., Hauksson, J. B., Davis, N. L., Pande, U., de Ropp, J. S., Langry, K. C., Smith, K. M., and La Mar, G. N. (1999) 1H NMR investigation of the role of intrinsic heme versus protein-induced rhombic perturbations on the electronic structure of low-spin ferrihemoproteins: Effect of heme substituents on heme orientation in myoglobin. *J. Am. Chem. Soc. 121*, 835−843.

(49) Hansch, C., Leo, A., and Taft, R. W. (1991) A survey of Hammett substituent constants and resonance and field parameters. *Chem. Rev. 91*, 165−195.

(50) La Mar, G. N., Toi, H., and Krishnamoorthi, R. (1984) Proton NMR Investigation of the Rate and Mechanism of Heme Rotation in Sperm Whale Myoglobin; Evidence for Intramolecular Reorientation about a Heme Two-Fold Axis. *J. Am. Chem. Soc. 106*, 6395−6401.

(51) Springer, B. A., Sligar, S. G., Olson, J. S., and Phillips, G. N. (1994) Mechanisms Of Ligand Recognition In Myoglobin. *Chem. Rev. 94*, 699−714.

(52) Liu, Y., and Ortiz de Montellano, P. R. (2000) Reaction Intermediates and Single Turnover Rate Constants for the Oxidation of Heme by Human Heme Oxygenase-1. *J. Biol. Chem. 275*, 5297−5307.

(53) Wang, J., and Ortiz de Montellano, P. R. (2003) The Binding Sites on Human Heme Oxygenase-1 for Cytochrome P450 Reductase and Biliverdin Reductase. *J. Biol. Chem. 278*, 20069−20076.